Published in final edited form as:
Circ Arrhythm Electrophysiol. 2016 December ; 9(12): . doi:10.1161/CIRCEP.115.003432.

Atrioventricular node dysfunction and ion channel transcriptome in pulmonary hypertension

Ian P. Temple, BSc, MBChB, MRCP, PhD[1,*], **Sunil Jit R.J. Logantha, BPharm, MSc, PhD**[1,*], **Mais Absi, PhD**[1], **Yu Zhang, BSc**[1], **Eleftheria Pervolaraki, BSc, MSc, PhD**[2], **Joseph Yanni, MB ChB, MSc, PhD**[1], **Andrew Atkinson, MBioMedSci, MPhil**[1], **Maria Petkova, BSc, MRes**[1], **Gillian M. Quigley, BSc, PhD**[1], **Simon Castro, MPhys, PhD**[3], **Mark Drinkhill, BSc, PhD**[2], **Heiko Schneider, MRCP, PhD**[1], **Oliver Monfredi, BSc, MBChB PhD**[1], **Elizabeth Cartwright, BSc, MSc, PhD**[1], **Min Zi, MD, MPhil**[1], **Tomoko T. Yamanushi, BSc, MS, PhD**[4], **Vaikom S. Mahadevan, MBBS, MD, FRCP, FACC**[5], **Alison M. Gurney, BSc, PhD, FRSB, FBPhS**[1], **Ed White, BSc, PhD**[2], **Henggui Zhang, BSc, MSc, PhD**[3], **George Hart, MA, DM, FRCP, FACC**[1], **Mark R. Boyett, BSc, PhD, FSB, FRCP**[1,†], and **Halina Dobrzynski, BSc, PhD**[1,†]

[1]Cardiovascular Sciences, University of Manchester, Manchester, UK

[2]School of Biomedical Sciences, University of Leeds, Leeds, UK

[3]School of Physics and Astronomy, University of Manchester, Manchester, UK

[4]Kagawa Prefectural College of Health Sciences, Takamatsu, Japan

[5]Department of Medicine, University of California, San Francisco, USA

Abstract

Background—Heart block is associated with pulmonary hypertension and the aim of the study was to test the hypothesis that the heart block is the result of a change in the ion channel transcriptome of the atrioventricular node.

Methods and Results—The most commonly used animal model of pulmonary hypertension, the monocrotaline-injected rat, was used. The functional consequences of monocrotaline injection were determined by echocardiography, ECG recording and electrophysiological experiments on the Langendorff-perfused heart and isolated atrioventricular node. The ion channel transcriptome was measured by quantitative PCR, and biophysically-detailed computer modelling was used to explore the changes observed. Following monocrotaline injection: echocardiography revealed the pattern of pulmonary artery blood flow characteristic of pulmonary hypertension as well as right-sided hypertrophy and failure; the Langendorff-perfused heart and isolated atrioventricular node revealed dysfunction of the atrioventricular node (e.g. 50% incidence of heart block in isolated AV node); and quantitative PCR revealed a widespread downregulation of ion channel and related genes in the atrioventricular node (e.g. >50% downregulation of $Ca_v1.2/3$ and HCN1/2/4

Corresponding author: Professor Mark Boyett; Cardiovascular Sciences, University of Manchester, Core Technology Facility, 46 Grafton Street, Manchester M13 9NT, UK; Tel: +44 161 275 1192 Fax: +44 161 275 1183, mark.boyett@manchester.ac.uk.
*Joint first authors
†Joint senior authors

Disclosures
None.

Europe PMC Funders Author Manuscripts

channels). Computer modelling predicted that the changes in the transcriptome if translated into protein and function would result in heart block.

Conclusions—Pulmonary hypertension results in a derangement of the ion channel transcriptome in the atrioventricular node and this is the likely cause of atrioventricular node dysfunction in this disease.

Keywords

Pulmonary hypertension; Arrhythmias; Atrioventricular node; Heart block; Ion channels

Journal Subject Terms

Arrhythmias; Animal Models of Human Disease; Ion Channels/Membrane Transport; Gene Expression and Regulation; Heart Failure; Pulmonary Hypertension

Introduction

Pulmonary arterial hypertension (PHT) is a disease characterised by raised pulmonary vascular resistance. It has a poor prognosis typically resulting in progressive right ventricular failure and death. The incidence of arrhythmias in patients with PHT is high.1–3 All forms of supraventricular tachycardia are more common in PHT with studies suggesting an incidence of ~3%/year and a prevalence of supraventricular arrhythmia of ~12%.3 Atrial flutter, atrial fibrillation and atrioventricular (AV) nodal reentrant tachycardia are common.3,4 There is evidence of AV node dysfunction in PHT with a 14% incidence of first degree heart block, a mean PR interval of 180±50 ms (mean±SD) and 2% of patients requiring a pacemaker for high degree heart block on initial screening of PHT patients.1 This can be compared with an incidence of first degree heart block of 2.1% and mean PR interval of 160±22 ms (mean±SD) for men and 153±22 ms (mean±SD) for women in the general population.5 Sleep apnoea causes PHT6 and is associated with heart block (heart block during sleep has been described in up to 10% of patients with obstructive sleep apnoea).7 Despite the evidence of a high burden of arrhythmias in patients with PHT, including dysfunction of the AV node, there is limited experimental data looking at the mechanisms of arrhythmia generation and the available data only concern arrhythmogenic mechanisms in the ventricle.e.g.8 There are several animal models of PHT, but the monocrotaline model is the best characterised and most widely used.e.g.9 Two studies using *in vivo* monitoring have demonstrated severe AV node dysfunction with heart block causing death in ~38% of monocrotaline-injected rats with PHT.10,11 In the present study, the monocrotaline-injected rat was chosen to study the mechanisms underlying AV node dysfunction in PHT (see Supplementary Material for further validation of the monocrotaline-injected rat model). We show that the dysfunction is associated with widespread remodelling of the ion channel transcriptome.

Methods

200 g male Wistar rats received an intraperitoneal injection of monocrotaline (60 mg/kg) or volume-matched 0.9% saline (3 ml/kg). Rats were weighed and their clinical condition

Europe PMC Funders Author Manuscripts

assessed twice weekly in the first 18 days and daily thereafter. Rats were assessed using echocardiography and ECG recording on day 0 immediately prior to injection, day 21 and immediately prior to termination. M-mode recordings were taken in the parasternal short axis view allowing recording of left ventricle anterior and posterior wall thickness and the internal diameter of the left ventricle in both systole and diastole. Right ventricle wall thickness was measured from M-mode recordings in the parasternal long axis view. Continuous wave Doppler recordings through the pulmonary artery were used to assess the pulmonary velocity profile. Monocrotaline-injected rats were sacrificed by stunning and cervical dislocation on day 28 or earlier if there was evidence of clinical deterioration (reduced movement, increased respiratory rate, piloerection, weight loss of >10 g over two days). A saline-injected rat was sacrificed within 24 h of sacrifice of a monocrotaline-injected rat. Heart and lungs were excised and weighed. Telemetric recordings of ECGs from conscious and unrestrained male Wistar rats were made as previously described by Benoist *et al.*12 The functioning of the AV node was measured in the Langendorff-perfused heart: the heart was mounted on a Langendorff column and retrogradely perfused with oxygenated Tyrode's solution at a temperature of 36.5°C. Extracellular electrodes were used to record a 'pseudo-ECG'. RR, PR and QT intervals and QRS duration were measured. Pacing protocols were performed to measure atrial and ventricular effective refractory periods, AV node refractory periods and Wenckebach cycle length. Functioning of the AV node was also measured in the isolated AV node: a preparation was placed in a perfusion bath with oxygenated Tyrode's solution at 36.5°C. Extracellular electrodes were used to record signals in the atrium and at the His bundle. Pacing protocols were performed to measure AV node refractory periods and Wenckebach cycle length. From the isolated AV node, intracellular actions potentials were also recorded with sharp microelectrodes.

Tissue was microdissected from different regions of the AV node: the AV node was sectioned at 50 μm in a cryostat. Sections 300 μm apart were stained with Masson's trichrome and immunolabelled for HCN4 and Cx43 to identify AV node tissues. Guided by this, AV node tissues were dissected with a sharp needle from remaining sections (haematoxylin and eosin stained). Total RNA was extracted using the MirVana kit, residual genomic DNA removed using TurboDNAse, RNA in each sample measured using the Qubit system, RNA reverse transcribed to produce cDNA using SuperScript VILO Mastermix with random hexamers, cDNA preamplified, and expression of different cDNAs corresponding to different mRNAs quantified using the TaqMan low density array card system (Life Technologies, USA). Expression was normalised to the abundance of a pair of housekeeper genes, B2M and PKG1, selected from 16 potential housekeeper genes as the most stable. The limma statistical package as implemented by RealTime Statminer software (Integromics) was used to compare mRNA expression in the control and monocrotaline-injected rats as well as compare mRNA expression in the different parts of the AV node. Multiple comparisons in large bodies of data, such as in microarray data analysis, pose statistical challenges.13,14 Typically, a correction is made when making multiple tests to avoid false-positive results (type I error),13,14 but reducing the type I error increases the chance of false-negative results (type II error).13,14 In relation to large data sets, Rothman14 has argued that a policy of not making corrections for multiple tests is preferable. For comparison of mRNA expression in the control and monocrotaline-injected

rats, the uncorrected *P* value is given in Table S3. Even without the argument from Rothman, 14 this can be justified, because each comparison is independent of the others (the conclusions of the present study do not depend on a group of differences being significant). Nevertheless, false discovery rate (FDR)-corrected *P* values are also given in Table S3 - multiple test corrections of the classical type are not commonly used in the analysis of microarray data and instead the FDR has become a standard for multiple tests correction.13 In reporting both uncorrected and FDR-corrected *P* values from the limma test, we follow the example of earlier studies.15,16 In Figs. 4-7, however, for simplicity the asterisks relate only to the FDR-corrected *P* value; cases in which the FDR-corrected *P* value is less than 0.2 (i.e. 20%) are highlighted with asterisks. An FDR of 20% (as we have used previously16) is permissive and means that ~20% of the 77 changes highlighted by asterisks, i.e. ~15, are false-positives. However, precise uncorrected and FDR-corrected *P* values are reported in Table S3 and the reader can make their own choice of what is acceptable. Rothman14 states that “scientists should not be so reluctant to explore leads that may turn out to be wrong that they penalize themselves by missing possibly important findings”. For comparison of mRNA expression in the different parts of the AV node, we report only FDR-corrected *P* values of <0.2 (using lower case letters) and <0.05 (using upper case letters) in Figs. 4-7, corresponding to false discovery rates of 20% and 5%. In this case, expression in various tissues is being compared and a multiple test correction is appropriate and we do not report uncorrected *P* values.

The potential consequences of the changes in transcripts were explored using a biophysically-detailed one-dimensional model (52.5 mm in length) consisting of segments of atrium (15 mm), AV node (12.5 mm), Purkinje fibre (20 mm) and ventricle (10 mm), each represented by a well-established model of the corresponding action potential. To simulate the functional effects of PHT, the conductance of each ionic current was scaled based on the change in the corresponding mRNA. The 1D cable equation was solved using the Forward-Time Central-Space scheme with a space step of 0.1 mm and time step of 0.005 ms. Finally, expression of protein was investigated using immunohistochemistry. See Supplementary Material for expanded methods.

Results

PHT and right-sided heart failure

There was no significant difference in the body weight of control (saline-injected) and monocrotaline-injected rats on the day of injection (Table 1). During the following three weeks, the monocrotaline-injected rats gained significantly less weight such that they weighed 12% less than the control rats by the day of termination (Table 1). Despite the lower body weight, the monocrotaline-injected rats also had a 23% increase in heart weight and an 88% increase in lung weight compared to the control group (Table 1). The heart:body weight and lung:body weight ratios were significantly greater in the monocrotaline-injected rats on the day of termination suggestive of congestive heart failure (Table 1). Previous studies of the monocrotaline model using echocardiography have demonstrated a characteristic change in the pulmonary artery velocity profile from the typical rounded shape to a ‘spike and dome’ morphology with a reduced pulmonary artery acceleration time (PAAT) and an

increased pulmonary artery deceleration (PAD) as pulmonary artery pressure increases.17,18 In the present study, PAAT and PAD were used as surrogate measures of pulmonary artery pressure. On the day of termination, echocardiography demonstrated a reduced PVAT and increased PAD in the monocrotaline-injected rats (Fig. 1B; Table 1). This is evidence of PHT and monocrotaline-injected rats will now be referred to as PHT rats. There was evidence of right-sided heart failure in the PHT rats: there was right ventricular dilatation (increased right ventricular internal dimension) and hypertrophy (increased right ventricular diastolic wall thickness) and a 36% reduction in right ventricular fractional shortening (Fig. 1A; Table 1). In contrast, in the left ventricle there was no evidence of hypertrophy and there was a *reduced* left ventricular internal diameter in the PHT rats - this was presumably the result of the raised right ventricular pressure pushing the ventricular septum into the left ventricle (Fig. 1A; Table 1). On the day of termination, the ECG measured *in vivo* in the anaesthetised rat showed a 98% increase in the QT interval, a 90% increase in the corrected QT interval (QTc interval) and a 9% increase in the RR interval (equivalent to 9% decrease in heart rate) in the PHT rats (Table 1); these changes are typical of heart failure.19 Although no changes were seen in the PR interval (Table 1), the PR interval is determined by the position of the leading pacemaker site in the right atrium as well as the conduction velocity of the AV node. We have previously reported similar changes in the ECG measured *in vivo* in the conscious rat using telemetry.12 In the UK, the Animal (Scientific Procedures) Act 1986 requires that monocrotaline-injected rats are sacrificed before they reach end-stage heart failure. However, one conscious freely-moving rat implanted with a telemetry system died naturally 28 days after injection with monocrotaline and the ECG recording showed that it died of heart block (Fig. 1C). This is consistent with earlier reports.10,11

Evidence from *in vitro* experiments of AV node dysfunction

It is possible that the AV node is supported *in vivo* by neurohumoral influences and, therefore, experiments were conducted on isolated heart preparations. First, experiments were conducted on the isolated Langendorff-perfused heart from 10 control and 11 PHT rats. Consistent with the *in vivo* measurements, there was a 141% increase in the QT interval, a 138% increase in QTc interval and a 144% increase in the ventricular effective refractory period in the PHT rats (Table 2). There was also a 24% increase in the atrial effective refractory period, but this was not significant (Table 2). Once again there was no change in the PR interval, but there was evidence of AV node dysfunction in the PHT rats: Fig. 2A shows typical AV node conduction curves from control and PHT rats – there was a significant increase in both the AV node effective and functional refractory periods (AVERP and AVFRP, respectively). The Wenckebach cycle length was increased (but not significantly) in the PHT rats. Although this increase was not significant, linear regression showed the Wenckebach cycle length to be significantly correlated with both the AVERP and AVFRP and this suggests that PHT does tend to prolong the Wenckebach cycle length (Fig. 2B). Experiments were also conducted on an isolated right atrial preparation containing the AV node from 10 control and 11 PHT rats. Electrograms were recorded from above the His bundle and examples are shown in Fig. 2C – both atrial and His bundle electrograms were recorded at the recording site. There was normal AV node conduction in the control rat, but complete heart block in the PHT rat with dissociation of the atrial and His bundle electrograms (Fig. 2C). There was a 50% incidence of complete heart block in the PHT rats

(6 of 12 PHT rats) compared to 0% in the control group (0 of 10 control rats); the difference is statistically significant (Fisher's exact test; P=0.015; Table 2). In the remaining 6 PHT rat preparations in which AV node conduction persisted, there were increases in the AH interval (interval between atrial and His bundle electrograms), the Wenckebach cycle length and the AVERP and AVFRP (at two drive train cycle lengths), although the increases did not reach significance (Table 2). Finally, using sharp microelectrodes, intracellular action potentials were recorded from isolated right atrial preparations from a further 5 control and 6 PHT rats, because this technique allows the well-known electrical heterogeneity of the AV node20 to be explored (Fig. 3). The preparations were paced from the region of the sinus node at 5 Hz. Normal AV node conduction was observed in 4 out of the 5 control preparations, whereas *abnormal* conduction was observed in 5 out of the 6 PHT preparations (Table S1). In PHT preparations, Fig. 3B shows an example of complete conduction block in the compact node (the action potentials show no correspondence to the stimulation artefacts and are spontaneous) and Fig. 3C shows a case of decremental conduction in the penetrating bundle. Taken together these data show evidence of AV node dysfunction in the PHT rat.

Remodelling of AV node

To understand the mechanisms underlying AV node dysfunction in PHT, the expression of ion channels, connexins, intracellular Ca^{2+}-handling proteins, ion pumps and exchangers and autonomic receptors was measured at the mRNA level using qPCR from 8 control and 8 PHT rats. Tissue was microdissected from four different regions of the AV node (transitional tissue, inferior nodal extension, compact node and penetrating bundle – Fig. 4 inset21 and Fig. S1 in Supplementary Material) as well as nearby atrial and ventricular muscle and total RNA was extracted from the different samples. Figs. 4-7 show the expression of many of the mRNA targets and Figs. S3-S6 show the expression of the remainder normalised to a housekeeper combination (B2M and PKG1). There are many significant differences in expression between different regions of the AV node, but for brevity are not discussed here. There are many significant differences in expression (generally downregulation) caused by PHT and these are considered below.

Downregulation of inward current carrying ion channels

In the AV node, inward current carrying ion channels play a role in diastolic depolarization, setting excitability and the upstroke and plateau of the action potential. HCN channels play an important role in pacemaking. HCN4 was the most abundant isoform and there was a trend of downregulation (significant in two regions) in the AV node in PHT (Fig. 4). $Na_v1.1$ is a subsidiary Na^+ channel involved in pacemaking and the action potential upstroke and again there was a trend of downregulation (significant in one region) in the AV node in PHT (Fig. 4). However, $Na_v1.5$ and $Na_v\beta1$ are responsible for the principal Na^+ channel in the heart and they were unaffected (Fig. 4). $Na_v1.8$ is responsible for the late Na^+ current;22 its expression in the AV node was unaffected in PHT, but interestingly its expression level was high in the penetrating bundle (Fig. S3). $Ca_v1.2$ and $Ca_v1.3$ are L-type Ca^{2+} channels and $Ca_v3.1$ and $Ca_v3.2$ are T-type Ca^{2+} channels and all are involved in pacemaking and the action potential upstroke. There was a trend for all the Ca^{2+} channels to be downregulated (but only significant in some cases) in the AV node in PHT (Figs. 4 and S4). However, there were no changes in three Ca^{2+} channel accessory subunits ($Ca_v\alpha2\delta1$, $Ca_v\alpha2\delta2$ and $Ca_v\beta2$;

Fig. S4). CLC-3 is a volume-regulated Cl^- channel23 and it was significantly downregulated in the inferior nodal extension (Fig. S3). Another Cl^- channel, CLC-2, involved in pacemaking23 was unaffected (Fig. S3). The downregulation of these ion channel transcripts in the AV node in PHT could potentially compromise AV node conduction by affecting excitability and the action potential upstroke.

Downregulation of outward current carrying ion channels

Voltage-gated K^+ channels play an important role in action potential repolarization. The voltage-gated K^+ channel subunits responsible for the transient outward K^+ current ($K_v1.4$, $K_v4.2$, $K_v4.3$, KChIP2) and delayed rectifier K^+ current ($K_v1.2$, $K_v1.5$, $K_v2.1$, ERG1, K_vLQT1, minK) tended to be downregulated (significantly in some cases) in the AV node in PHT (Figs. 5 and S3). There were three significant decreases in inward rectifier K^+ channels in the AV node in PHT: $K_{ir}3.1$ (subunit of ACh-activated K^+ channel) in the transitional tissue, $K_{ir}3.4$ (another subunit of ACh-activated K^+ channel) in the inferior nodal extension and $K_{ir}6.2$ (subunit of ATP-sensitive K^+ channel) in the transitional tissue (Fig. 6). The twin pore K^+ channel, TWIK1, was significantly downregulated in the inferior nodal extension in the AV node in PHT (Fig. 6). The downregulation of the K^+ channels is expected to prolong the AV node action potential although such an effect would be countered by the downregulation of inward current carrying ion channels.

Downregulation of intracellular Ca^{2+}-handling molecules

Intracellular Ca^{2+} plays an important role in pacemaking and conduction in the AV node. 24,25 Expression of many intracellular Ca^{2+}-handling molecules was affected in PHT. There tended to be a downregulation of NCX1 (Na^+-Ca^{2+} exchanger) in the AV node in PHT, but this was not significant (Fig. 7). There was a tendency for RyR2 (the Ca^{2+} release channel of the sarcoplasmic reticulum - SR) to be downregulated in most tissues in PHT and it was significantly downregulated in the inferior nodal extension (Fig. 7). Although expression of SERCA2 in the AV node was not affected in PHT, two regulators of SERCA2 (phospholamban and sarcolipin) were significantly downregulated in much of the AV node (Fig. 7). Two other Ca^{2+}-handling molecules, calsequestrin 2 and PMCA1, were unaffected (Figs. 7 and S3). The downregulation of RyR2 could potentially slow AV node conduction.

Downregulation of other transcripts

In PHT, there was a trend of downregulation of the α2 and α3 subunits of the Na^+-K^+ pump throughout the AV node (significantly in some cases; Fig. S5). However, the α1 and β1 subunits were unchanged (Fig. S5). The Na^+-H^+ exchanger (NHE1) was significantly upregulated in the inferior nodal extension in PHT (Fig. S3). Connexins are responsible for electrical coupling between myocytes and therefore are an important determinant of conduction velocity of the action potential. No changes were seen in Cx40, Cx43 and Cx45 in any of the nodal tissues (Fig. 7). However, Cx30.2 has been suggested to play a key role in nodal tissues26 and it was significantly downregulated in both the transitional tissue and inferior nodal extension in PHT (Fig. 7). The AV node is controlled by the autonomic nervous system. Although there were no changes in the M2 muscarinic and A1 adenosine receptors in the AV node in PHT, there were changes in adrenergic receptors: there was a significant downregulation in the α1a/1c adrenergic receptor in the inferior nodal extension

and importantly there was a significant downregulation of the β1 receptor (the most important adrenergic receptor) in the inferior nodal extension (Fig. S6). There were no significant changes in two other adrenergic receptors (α1b and β2; Fig. S6). The downregulation of the β1 adrenergic receptor could negatively impact AV node conduction.

Remodelling predicts heart block

The significant changes in transcripts in the AV node in PHT in the present study are summarised in Tables S2 and S3. Biophysically-detailed action potential models have been used to predict *possible* changes in electrical activity based on changes in ion channel transcripts – ionic conductances are scaled depending on changes in mRNA (Supplementary Material). This should be viewed as a form of bioinformatics. Based on a biophysically-detailed one-dimensional (1D) model of the conduction pathway from the atrium through the AV node and Purkinje fibres to the ventricle,27 Fig. 8 shows the predicted effects of PHT-induced ion channel remodelling; the assumed changes in ionic conductances (based on expression of corresponding mRNAs) are shown in Table S11. In control conditions, the action potential is predicted to conduct from the atrium to the ventricle (Fig. 8A) and the conduction velocity (Fig. 8B) and action potential waveform (Fig. 8C) in the different tissues are as expected. However in PHT, conduction is predicted to fail in the compact node (heart block; Fig. 8) consistent with Figs. 2 and 3. Of the changes in ion channels in PHT, the computer modelling predicts that the downregulation of the L-type Ca^{2+} channels, $Ca_v1.2$ and $Ca_v1.3$, is the most important. The expected downregulation of $I_{Ca,L}$ in the N region alone is sufficient to cause heart block (data not shown).

Discussion

This study is the first to demonstrate widespread downregulation of the ion channel transcriptome in the AV node in response to a disease process. Previously, AV node disease has been commonly attributed to idiopathic fibrosis and sclerosis.e.g.28 However, there are other recent data pointing to the importance of ion channels in normal AV conduction. A genome wide association study has demonstrated several loci that are associated with a prolonged PR interval, including genes for ion channels and developmental genes known to be important for the patterning of ion channels during embryogenesis.29 There is also a recognition that several disease-causing ion channel mutations that have been characterised as causing Brugada syndrome and long-QT syndrome are also associated with conduction system disturbances and heart block.19 In addition to these findings in patients, gene knockout studies in mice have pointed to the importance of several ion channels including voltage-dependent Ca^{2+} channelse.g.30 and HCN431 in maintaining normal AV conduction.

Dysfunction and remodelling of AV node in PHT

There was evidence of dysfunction of the AV node in the PHT rats: in the Langendorff-perfused heart, there was evidence of an increase in the AVERP, AVFRP and Wenckebach cycle length and, in the isolated AV node, there was a 50% incidence of complete heart block (Fig. 3). In one case, in which a PHT rat died with a telemetry system fitted, it died of heart block (Fig. 1C) and this is consistent with earlier telemetric studies;10,11 for example, Chi *et al.*11 reported that ~38% of PHT (monocrotaline-injected) rats die of heart block.

There was a widespread downregulation in the ion channel transcriptome in the AV node in PHT (Tables S2 and S3). AV node conduction will be potentially slowed by the downregulation of many of the transcripts and computer modelling confirmed that if the changes in mRNA are translated into changes in function they will result in heart block (Fig. 8). The potential role played by the downregulation of some transcripts will be briefly discussed.

Primary role for Ca^{2+} channels

The upstroke and conduction of the action potential of the AV node is known to be dependent on L-type Ca^{2+} channels. For example, knockout of either $Ca_v1.2$ and $Ca_v1.3$ has been reported to slow or block AV node conduction.32,33 A downregulation of $Ca_v1.2$ and $Ca_v1.3$ was observed in the AV node in PHT (Fig. 4) and the computer modelling predicts that the expected decrease in L-type Ca^{2+} current alone is sufficient to cause heart block. We suggest that this is the primary cause of AV node dysfunction in PHT.

The T-type Ca^{2+} channels, $Ca_v3.1$ and $Ca_v3.2$, also tended to decrease (Figs. 4 and S4) and knockout of $Ca_v3.1$ at least has been shown to slow AV node conduction.30 RyR2 was significantly downregulated in the AV node in PHT (Fig. 7). RyR2 is an important part of the Ca^{2+} clock. The 'Ca^{2+} clock' as well as the 'membrane clock' (the principal component of which is the funny current, I_f) controls pacemaking in the sinus and AV nodes.24 However, there is also evidence that it controls AV node conduction: Saeed *et al.*25 have shown that incapacitating RyR2 and the Ca^{2+} clock by application of ryanodine slows AV node conduction. The Ca^{2+} clock could control AV node conduction by affecting excitability and, therefore, the downregulation of RyR2 in PHT may be important. Further components of the Ca^{2+} clock tended to be downregulated in the AV node in PHT (Fig. 7), markedly in the case of phospholamban and sarcolipin; the consequences of these changes for AV node conduction are unknown.

Role for downregulation of HCN4?

Downregulation of the HCN4 channel in the AV node was observed in PHT (Fig. 4; see also Fig. S8). HCN channels and I_f (inward current during diastole that is responsible for phase 4 depolarization) have mainly been considered in relation to sinus node pacemaking. Indeed an I_f blocking drug, ivabradine, is used clinically to reduce sinus rate. Initial studies on a small number of patients demonstrated no effects on the AV node and therefore subsequent larger studies have not investigated the effects of ivabradine on the AV node.e.g.34 However, there are several recent studies that suggest that I_f may play a significant role in AV node conduction. This study has demonstrated high levels of HCN4 in the AV node (Fig. 4). There is also functional evidence that I_f plays a role in AV node conduction: although ivabradine was not shown to have an effect on the human AV node, another I_f blocking agent, zatebradine, has been shown to increase the AH interval, AVERP and Wenckebach cycle length in humans.35 Ivabradine has also been shown to slow the ventricular response to atrial fibrillation in dogs with the mechanism thought to be specific to I_f blockade within the AV node slowing conduction and not a direct effect of I_f blockade on the atrium.36 Inducible cardiac specific knockout of HCN4 in mice is lethal because of the development of complete heart block.31 Saeed *et al.*25 have shown that in young rats I_f block significantly

prolongs the AH interval, AVERP and Wenckebach cycle length. Downregulation of I_f could slow AV node conduction by decreasing excitability of the cell.37

Role for other factors?

A downregulation of various K^+ channels was observed in the AV node in PHT (Figs. 5 and 6). This is not surprising, because in the ventricles a downregulation of K^+ channels has been shown in a number of different disease models including PHT.38 In the ventricles, the downregulation leads to a prolongation of the action potential.38 In the present study, it has not been highlighted, but many K^+ channels were downregulated in both the atrial and ventricular working myocardium (Figs. 5, 6 and S3) and the functional experiments demonstrated an increased VERP and suggested an increased AERP, which is consistent with an increase in action potential duration. The downregulation of K^+ channels in the AV node could explain the observed increase in AVERP, AVFRP and Wenckebach cycle length in PHT (Fig. 2). In the transitional tissue at least, the computer modelling predicts a prolongation of the AV node action potential in PHT (Fig. 8). Regan *et al.*39 observed that selective pharmacological block of ERG ($I_{K,r}$) and K_vLQT1 ($I_{K,s}$) both cause a prolonged AH interval and AVERP in rats. Although ERG and K_vLQT1 were unaffected by PHT (Fig. 5), this demonstrates that K^+ channels are able to affect AV node conduction and refractoriness. Recently, Mesirca *et al.*40 reported that ablation of the ACh-activated K^+ current (carried by $K_{ir}3.1$ and $K_{ir}3.4$) relieves the heart block in $Ca_v1.3$ knockout mice. In PHT, $K_{ir}3.1$ and $K_{ir}3.4$ tended to be downregulated in PHT and this could be a compensatory mechanism. Changes in K^+ channels could potentially alter the membrane potential during diastole and this would have indirect consequences, for example for the Na^+ current. The only connexin that was significantly affected within the nodal tissue was Cx30.2, which was downregulated (Fig. 7). However, paradoxically, knockout of the very low conductance Cx30.2 leads to an increased conduction velocity across the AV node.41

Cardiac sympatholysis

Activation of the sympathetic nervous system and an increase in plasma norepinephrine levels is a feature of heart failure.42 In keeping with this, Leineweber *et al.*43 showed that, in the monocrotaline-injected rat, plasma norepinephrine levels are markedly increased. The activation of the sympathetic nervous system can support the failing heart (although it can also be detrimental to the heart and cause hypertrophy for example).42 In the present study, whereas AV node function was generally normal *in vivo* (Table 1), AV node function was worse in the Langendorff-perfused heart (AVERP and AVFRP were significantly longer; Table 2) and it was worse again in the isolated right atrial preparation (when conduction block was frequently observed; Figs. 2 and 3 and Tables 2 and S1). This is consistent with dysfunction of the AV node in PHT and *in vivo* the failing AV node being supported by the activation of the sympathetic nervous system.

In heart failure, the elevated norepinephrine levels are known to result in downregulation of β-receptors as a result of desensitization.42 In the monocrotaline-injected rat, Leineweber *et al.*43 showed that there is a downregulation of β-receptors at the protein level and a diminished responsiveness to β-stimulation. The data from the present study are consistent with this. In the rat, of the β1- and β2-receptors, the β1-receptor is the dominant isoform43

and the same is true in the present study at the mRNA level (Fig. S6). In the present study, there tended to be a downregulation of β-receptors in the PHT rats (although the downregulation was only significant in some regions; Fig. S6). Interestingly, in the present study, there was also a downregulation of a-receptors at the mRNA level in some regions (Fig. S6); Leineweber *et al.*43 also reported a downregulation. In a pilot experiment, sympathetic nerve fibres in the AV node were immunolabelled using an antibody to neurofilament 150;44 dense innervation was observed, but there was no marked change in PHT (Fig. S7). The consequences of these changes can only be speculated on. The downregulation of β-receptors in PHT could contribute to failure of the AV node *in vivo* (because activation of the sympathetic nervous system would no longer be able to support the failing AV node).

Clinical implications

Heart block is a common condition in both PHT and the general population and is the indication for over half of implanted pacemakers.45 AV node disease has typically been attributed to fibrosis, but this study shows that this is not necessarily the case. This study shows that in PHT it is more likely to be the result of remodelling of the ion channel transcriptome. In this respect, the AV node is no different from the rest of the heart – in heart disease, there is a well-known remodelling of the ion channel transcriptome in the sinus node and working myocardium. Recognition of the causes of AV node disease is the first step to developing new treatments.

Further discussion of the findings can be found in the Supplementary Material.

Supplementary Material

Refer to Web version on PubMed Central for supplementary material.

Sources of funding

Work undertaken with support of a Clinical Research Fellowship (FS/10/69/28495) and a programme grant (RG/11/18/29257) from the British Heart Foundation.

References

1. Bossone E, Paciocco G, Iarussi D, Agretto A, Iacono A, Gillespie BW, Rubenfire M. The prognostic role of the ECG in primary pulmonary hypertension. Chest. 2002; 121:513–518. [PubMed: 11834666]
2. Kanemoto N, Sasamoto H. Arrhythmias in primary pulmonary hypertension. Jpn Heart J. 1979; 20:765–775. [PubMed: 522240]
3. Tongers J, Schwerdtfeger B, Klein G, Kempf T, Schaefer A, Knapp JM, Niehaus M, Korte T, Hoeper MM. Incidence and clinical relevance of supraventricular tachyarrhythmias in pulmonary hypertension. Am Heart J. 2007; 153:127–32. [PubMed: 17174650]
4. Ruiz-Cano MJ, Gonzalez-Mansilla A, Escribano P, Delgado J, Arribas F, Torres J, Flox A, Riva M, Gomez MA, Saenz C. Clinical implications of supraventricular arrhythmias in patients with severe pulmonary arterial hypertension. Int J Cardiol. 2011; 146:105–6. [PubMed: 21056484]
5. Aro AL, Anttonen O, Kerola T, Junttila MJ, Tikkanen JT, Rissanen HA, Reunanen A, Huikuri HV. Prognostic significance of prolonged PR interval in the general population. Eur Heart J. 2014; 35:123–9. [PubMed: 23677846]

6. Laks L, Lehrhaft B, Grunstein RR, Sullivan CE. Pulmonary hypertension in obstructive sleep apnoea. Eur Respir J. 1995; 8:537–41. [PubMed: 7664850]
7. Koehler U, Fus E, Grimm W, Pankow W, Schafer H, Stammnitz A, Peter JH. Heart block in patients with obstructive sleep apnoea: pathogenetic factors and effects of treatment. Eur Respir J. 1998; 11:434–9. [PubMed: 9551750]
8. Uzzaman M, Honjo H, Takagishi Y, Emdad L, Magee AI, Severs NJ, Kodama I. Remodeling of gap junctional coupling in hypertrophied right ventricles of rats with monocrotaline-induced pulmonary hypertension. Circ Res. 2000; 86:871–878. [PubMed: 10785509]
9. Stenmark KR, Meyrick B, Galie N, Mooi WJ, McMurtry IF. Animal models of pulmonary arterial hypertension: the hope for etiological discovery and pharmacological cure. Am J Physiol. 2009; 297:L1013–32.
10. Watkinson WP, Campen MJ, Costa DL. Cardiac arrhythmia induction after exposure to residual oil fly ash particles in a rodent model of pulmonary hypertension. Toxicol Sci. 1998; 41:209–16. [PubMed: 9520357]
11. Chi L, Liles J, Arolfo M, Oliver J, Dhalla A, Belardinelli L. Direct evidence of unprovoked arrhythmias in telemetered, conscious rats with chronic pulmonary artery hypertension. Am J Resp Crit Care. 2013; 187:A4648.
12. Benoist D, Stones R, Drinkhill MJ, Benson AP, Yang Z, Cassan C, Gilbert SH, Saint DA, Cazorla O, Steele DS, Bernus O, et al. Cardiac arrhythmia mechanisms in rats with heart failure induced by pulmonary hypertension. Am J Physiol-Heart C. 2012; 302:H2381–95.
13. Katagiri F. Multiple tests correction, false discovery rate and q value. Physiology News. 2009; 77:35–38.
14. Rothman KJ. No adjustments are needed for multiple comparisons. Epidemiology. 1990; 1:43–6. [PubMed: 2081237]
15. Myers SA, Eriksson N, Burow R, Wang SC, Muscat GE. Beta-adrenergic signaling regulates NR4A nuclear receptor and metabolic gene expression in multiple tissues. Mol Cell Endocrinol. 2009; 309:101–8. [PubMed: 19465082]
16. Yanni J, Tellez JO, Maczewski M, Mackiewicz U, Beresewicz A, Billeter R, Dobrzynski H, Boyett MR. Changes in ion channel gene expression underlying heart failure-induced sinoatrial node dysfunction. Circulation: Heart Failure. 2011; 4:496–508. [PubMed: 21565973]
17. Koskenvuo JW, Mirsky R, Zhang Y, Angeli FS, Jahn S, Alastalo TP, Schiller NB, Boyle AJ, Chatterjee K, De Marco T, Yeghiazarians Y. A comparison of echocardiography to invasive measurement in the evaluation of pulmonary arterial hypertension in a rat model. International Journal of Cardiovascular Imaging. 2010; 26:509–18. [PubMed: 20140524]
18. Urboniene D, Haber I, Fang YH, Thenappan T, Archer SL. Validation of high-resolution echocardiography and magnetic resonance imaging vs. high-fidelity catheterization in experimental pulmonary hypertension. Am J Physiol-Lung C. 2010; 299:L401–12.
19. Dobrzynski H, Anderson RH, Atkinson A, Borbas Z, D'Souza A, Fraser JF, Inada S, Logantha SJRJ, Monfredi O, Morris GM, Moorman AFM, et al. Structure, function and clinical relevance of the cardiac conduction system, including the atrioventricular ring and outflow tract tissues. Pharmacol Therapeut. 2013; 139:260–288.
20. Billette J. Atrioventricular nodal activation during periodic premature stimulation of the atrium. Am J Physiol. 1987; 252:H163–H177. [PubMed: 3812708]
21. Greener ID, Tellez JO, Dobrzynski H, Yamamoto M, Graham GM, Billeter R, Boyett MR. Ion channel transcript expression at the rabbit atrioventricular conduction axis. Circulation: Arrhythmia and Electrophysiology. 2009; 2:305–315. [PubMed: 19808481]
22. Yang T, Atack TC, Stroud DM, Zhang W, Hall L, Roden DM. Blocking Scn10a channels in heart reduces late sodium current and is antiarrhythmic. Circ Res. 2012; 111:322–32. [PubMed: 22723299]
23. Duan D. Phenomics of cardiac chloride channels: the systematic study of chloride channel function in the heart. J Physiol. 2009; 587:2163–77. [PubMed: 19171656]
24. Cheng H, Smith GL, Hancox JC, Orchard CH. Inhibition of spontaneous activity of rabbit atrioventricular node cells by KB-R7943 and inhibitors of sarcoplasmic reticulum Ca^{2+} ATPase. Cell Calcium. 2011; 49:56–65. [PubMed: 21163524]

25. Saeed Y, Temple IP, Borbas Z, Atkinson A, Yanni J, Boyett MR, Garratt C, Dobrzynski H. Do major ion channels of pacemaker clock play a role in AV nodal conduction in young and old rats? Eur Heart J. 2015; 36(Abstract Supplement):1121.
26. Kreuzberg MM, Schrickel JW, Ghanem A, Kim JS, Degen J, Janssen-Bienhold U, Lewalter T, Tiemann K, Willecke K. Connexin30.2 containing gap junction channels decelerate impulse propagation through the atrioventricular node. P Natl Acad Sci USA. 2006; 103:5959–64.
27. Inada S, Hancox JC, Zhang H, Boyett MR. One-dimensional mathematical model of the atrioventricular node including atrio-nodal, nodal, and nodal-his cells. Biophys J. 2009; 97:2117–2127. [PubMed: 19843444]
28. Bailey, S., Burkhardt, JD., Bhargava, M. Bradycardia. Handbook of Cardiac Electrophysiology. Natale, A., Marchlinski, F., editors. CRC Press; 2007. p. 51-60.
29. Pfeufer A, van Noord C, Marciante KD, Arking DE, Larson MG, Smith AV, Tarasov KV, Muller M, Sotoodehnia N, Sinner MF, Verwoert GC, et al. Genome-wide association study of PR interval. Nat Genet. 2010; 42:153–9. [PubMed: 20062060]
30. Marger L, Mesirca P, Alig J, Torrente A, Dubel S, Engeland B, Kanani S, Fontanaud P, Striessnig J, Shin HS, Isbrandt D, et al. Functional roles of $Ca_V1.3$, $Ca_V3.1$ and HCN channels in automaticity of mouse atrioventricular cells: insights into the atrioventricular pacemaker mechanism. Channels. 2011; 5:251–61. [PubMed: 21406960]
31. Baruscotti M, Bucchi A, Viscomi C, Mandelli G, Consalez G, Gnecchi-Rusconi T, Montano N, Casali KR, Micheloni S, Barbuti A, DiFrancesco D. Deep bradycardia and heart block caused by inducible cardiac-specific knockout of the pacemaker channel gene Hcn4. P Natl Acad Sci USA. 2011; 108:1705–10.
32. Foell JD, Best JM, Lei M, Balijepalli RC, Molkentin JD, Powers PA, McKinnon D, Kamp TJ. Targeted loss of cardiac L-type Ca^{2+} $Ca_V1.2$ Channels in adult mouse causes sinus node dysfunction, AV block and supraventricular tachycardias. Circulation. 2008; 118:S-436.
33. Matthes J, Yildirim L, Wietzorrek G, Reimer D, Striessnig J, Herzig S. Disturbed atrio-ventricular conduction and normal contractile function in isolated hearts from Cav1.3-knockout mice. N-S Arch Pharmacol. 2004; 369:554–562.
34. Swedberg K, Komajda M, Bohm M, Borer JS, Ford I, Tavazzi L. Rationale and design of a randomized, double-blind, placebo-controlled outcome trial of ivabradine in chronic heart failure: the Systolic Heart Failure Treatment with the I_f Inhibitor Ivabradine Trial (SHIFT). Eur J Heart Fail. 2010; 12:75–81. [PubMed: 19892778]
35. Chiamvimonvat V, Newman D, Tang A, Green M, Mitchell J, Wulffhart Z, Dorian P. A double-blind placebo-controlled evaluation of the human electrophysiologic effects of zatebradine, a sinus node inhibitor. J Cardiovasc Pharm. 1998; 32:516–20.
36. Verrier RL, Sobrado MF, Pagotto VP, Kanas AF, Machado AD, Varone BB, Sobrado LF, Nearing BD, Zeng D, Belardinelli L. Inhibition of I_f in the atrioventricular node as a mechanism for dronedarone's reduction in ventricular rate during atrial fibrillation. Heart Rhythm. 2013; 10:1692–7. [PubMed: 23933296]
37. Li J, Temple IP, Boyett MR. Theoretical study of the role of the funny current (I_f) and the background inward current (I_b) in atrioventricular nodal conduction. Computing in Cardiology. 2014; 41:865–868.
38. Benoist D, Stones R, Drinkhill M, Bernus O, White E. Arrhythmogenic substrate in hearts of rats with monocrotaline-induced pulmonary hypertension and right ventricular hypertrophy. Am J Physiol. 2011; 300:H2230–H2237.
39. Regan CP, Cresswell HK, Zhang R, Lynch JJ. Novel method to assess cardiac electrophysiology in the rat: characterization of standard ion channel blockers. J Cardiovasc Pharm. 2005; 46:68–75.
40. Mesirca P, Bidaud I, Briec F, Evain S, Torrente AG, Le Quang K, Leoni AL, Baudot M, Marger L, Chung You Chong A, Nargeot J, et al. G protein-gated IKACh channels as therapeutic targets for treatment of sick sinus syndrome and heart block. P Natl Acad Sci USA. 2016; 113:E932–41.
41. Temple IP, Inada S, Dobrzynski H, Boyett MR. Connexins and the atrioventricular node. Heart Rhythm. 2013; 10:297–304. [PubMed: 23085482]
42. Liang CS. Sympatholysis and cardiac sympathetic nerve function in the treatment of congestive heart failure. J Am Coll Cardiol. 2003; 42:549–51. [PubMed: 12906987]

43. Leineweber K, Seyfarth T, Abraham G, Gerbershagen HP, Heinroth-Hoffmann I, Ponicke K, Brodde OE. Cardiac beta-adrenoceptor changes in monocrotaline-treated rats: differences between membrane preparations from whole ventricles and isolated ventricular cardiomyocytes. J Cardiovasc Pharm. 2003; 41:333–42.

44. Trojanowski JQ, Walkenstein N, Lee VM. Expression of neurofilament subunits in neurons of the central and peripheral nervous system: an immunohistochemical study with monoclonal antibodies. J Neurosci. 1986; 6:650–60. [PubMed: 2420946]

45. Uslan DZ, Tleyjeh IM, Baddour LM, Friedman PA, Jenkins SM, St Sauver JL, Hayes DL. Temporal trends in permanent pacemaker implantation: a population-based study. Am Heart J. 2008; 155:896–903. [PubMed: 18440339]

Europe PMC Funders Author Manuscripts

Europe PMC Funders Author Manuscripts

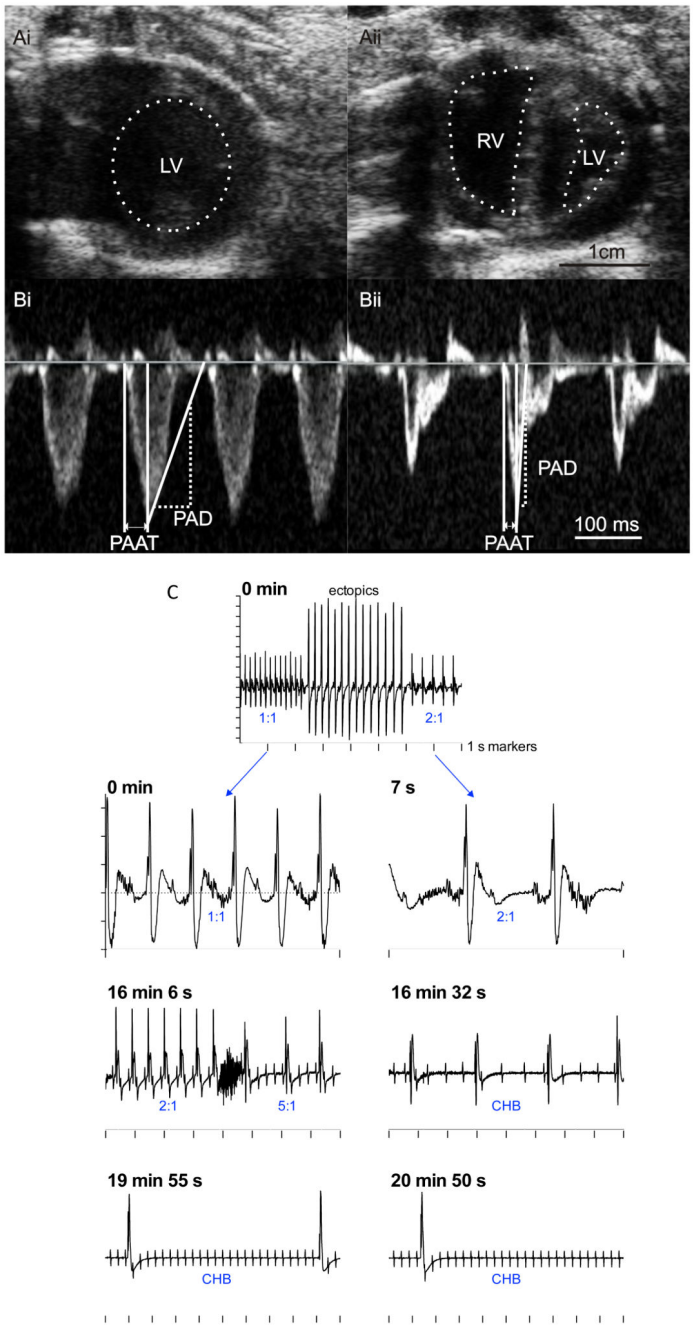

Fig. 1.

A and B, echocardiography images (on day 23 following monocrotaline injection) showing development of PHT. A, parasternal short axis view from control (Ai) and monocrotaline-injected (Aii) rats. The left and right ventricles (LV and RV) are identified by dotted lines (not possible to identify right ventricle in control rat). B, pulmonary velocity profile from control (Bi) and monocrotaline-injected (Bii) rats. Measurement of pulmonary artery acceleration time (PAAT) and pulmonary artery deceleration (PAD) shown. C, death of rat with PHT caused by complete heart block 28 days following monocrotaline injection. ECGs

recorded by telemetry at different times during final 21 min shown. Ratio of atrial to ventricular beats shown in blue. ECGs shown on different time bases (1 s time marks shown). Y-axis shows 0.2 mV increments. CHB, complete heart block.

Europe PMC Funders Author Manuscripts

Europe PMC Funders Author Manuscripts

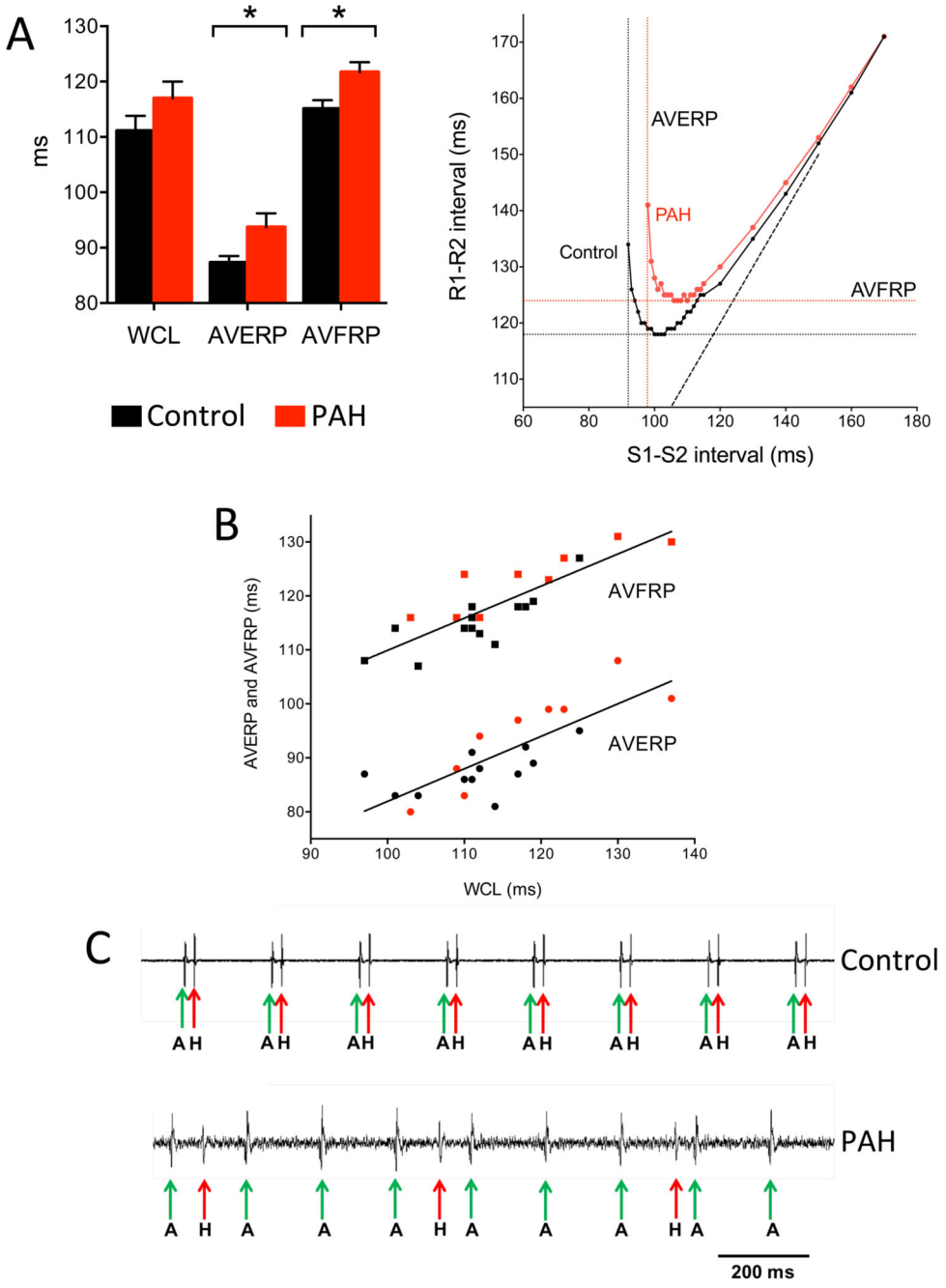

Fig. 2.

Impaired AV node conduction in PHT rats. All data collected on day of termination. A (left), mean (+SEM) Wenckebach cycle length (WCL), AVERP and AVFRP in control (black bars) and PHT (red bars) rats (n=10). Recordings made from Langendorff-perfused heart. **P*<0.05 (Student's t test). A (right), typical AV node conduction curves from control and PHT rats showing measurement of AVERP and AVFRP. B, significant correlation between AVERP and AVFRP and Wenckebach cycle length. Each point corresponds to different rat, control (black) or PHT (red). Data are fit by linear regression (AVERP, R^2=0.63, *P*<0.001; AVFRP,

R^2=0.71, P<0.0001). C, demonstration of complete heart block in PHT rat. Extracellular potential recordings from region of His bundle of control (top trace) and PHT (bottom trace) rats shown. Recordings made from isolated AV node. Atrial (labelled A and marked with green arrow) as well as His bundle (labelled H and marked with red arrow) signals recorded.

Europe PMC Funders Author Manuscripts

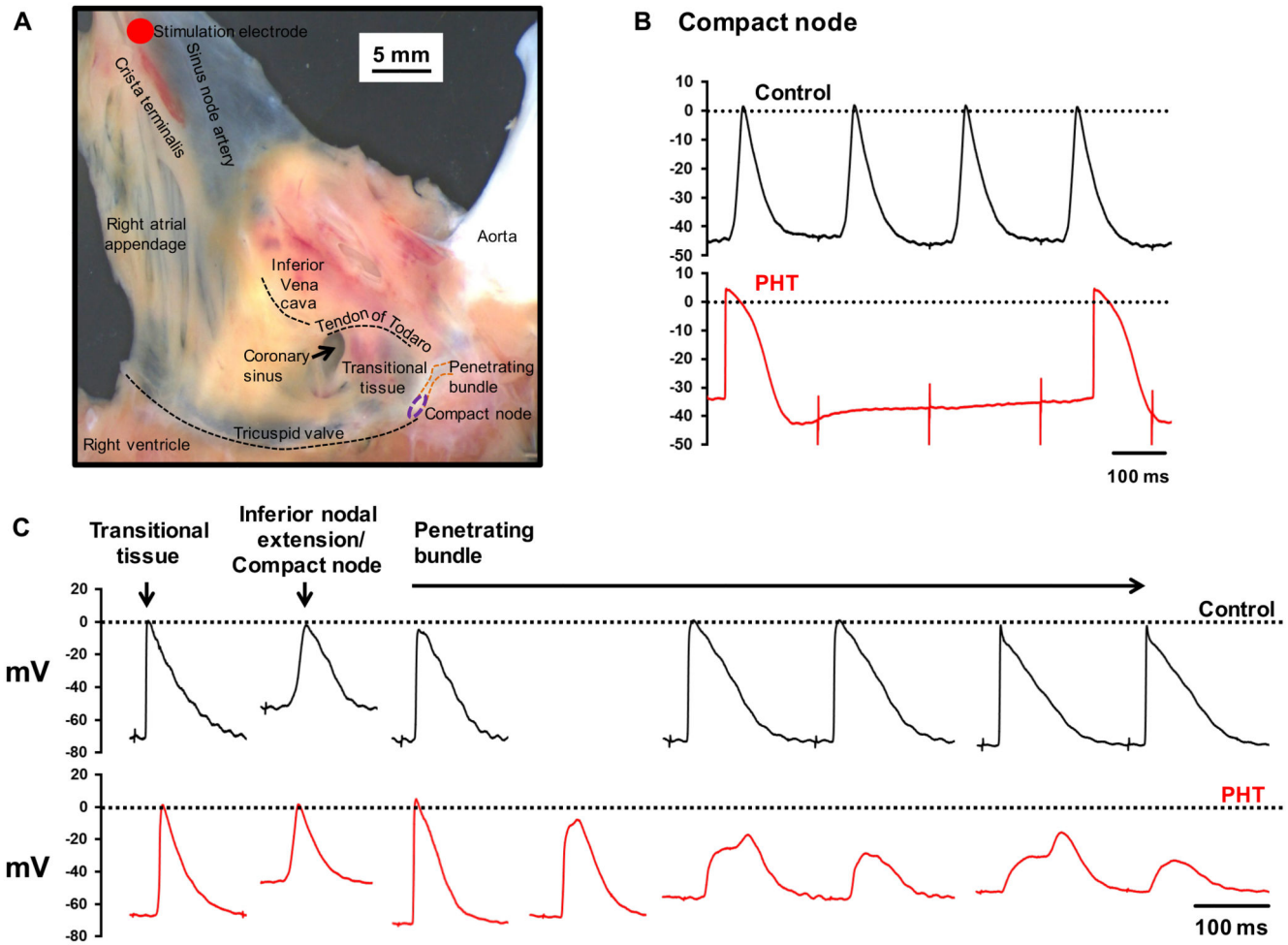

Fig. 3.

Heart block in PHT rats explored further. A, example of AV node preparation used for intracellular action potential recording. Tissue was paced at 5 Hz at level of sinus node. B, intracellular action potentials recorded from compact node showing normal 1:1 conduction in control preparation and complete heart block (as well as ectopic action potentials) in PHT preparation. Sharp deflections, stimulation artefacts. C, intracellular action potentials recorded along AV conduction axis (transitional tissue, inferior nodal extension/compact node and penetrating bundle) showing normal conduction in control preparation and decremental conduction in penetrating bundle in PHT preparation.

Europe PMC Funders Author Manuscripts

Europe PMC Funders Author Manuscripts

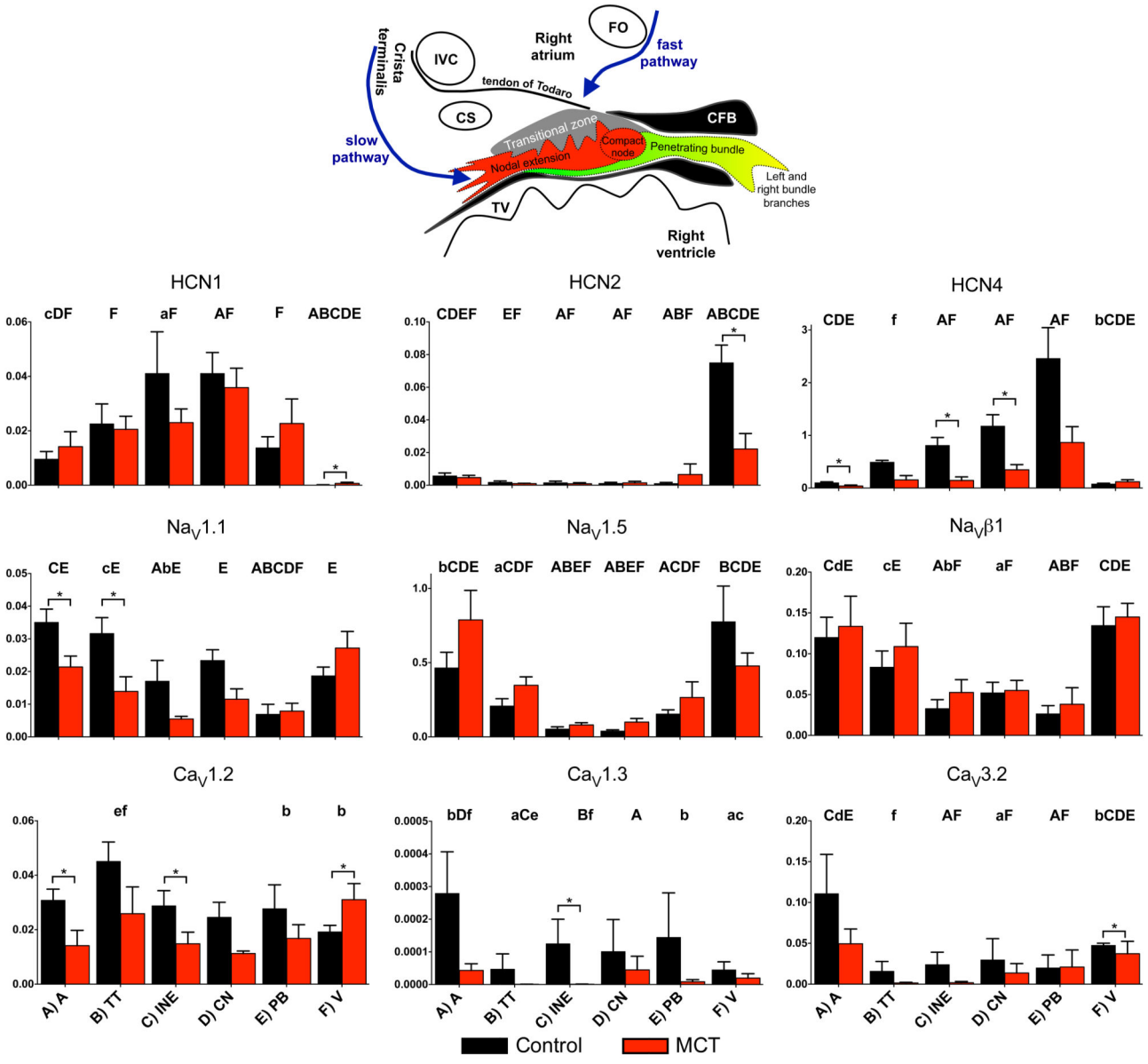

Fig. 4.

Expression of mRNA for ion channels carrying inward current. In this and similar figures: expression shown in atrial muscle (A; A), transitional tissue (B; TT), inferior nodal extension (C; INE), compact node (D; CN), penetrating bundle (E; PB) and ventricular muscle (F; V) from control (black bars) and PHT (red bars) rats; means (+SEM) shown (n=6-8); bars and asterisks indicate significant differences between control and PHT rats as assessed by the limma test (FDR-corrected P<0.2, i.e. 20%); and, for the control tissues only, letters indicate a significant difference from the appropriately lettered region (lower case letters, FDR-corrected P<0.2, i.e. 20%; upper case letters, FDR-corrected P<0.05, i.e. 5%). Inset, schematic diagram of AV node (from Greener *et al.*21). CFB, central fibrous body; CS, coronary sinus; IVC, inferior vena cava; FO, fossa ovalis; TV, tricuspid valve.

Europe PMC Funders Author Manuscripts

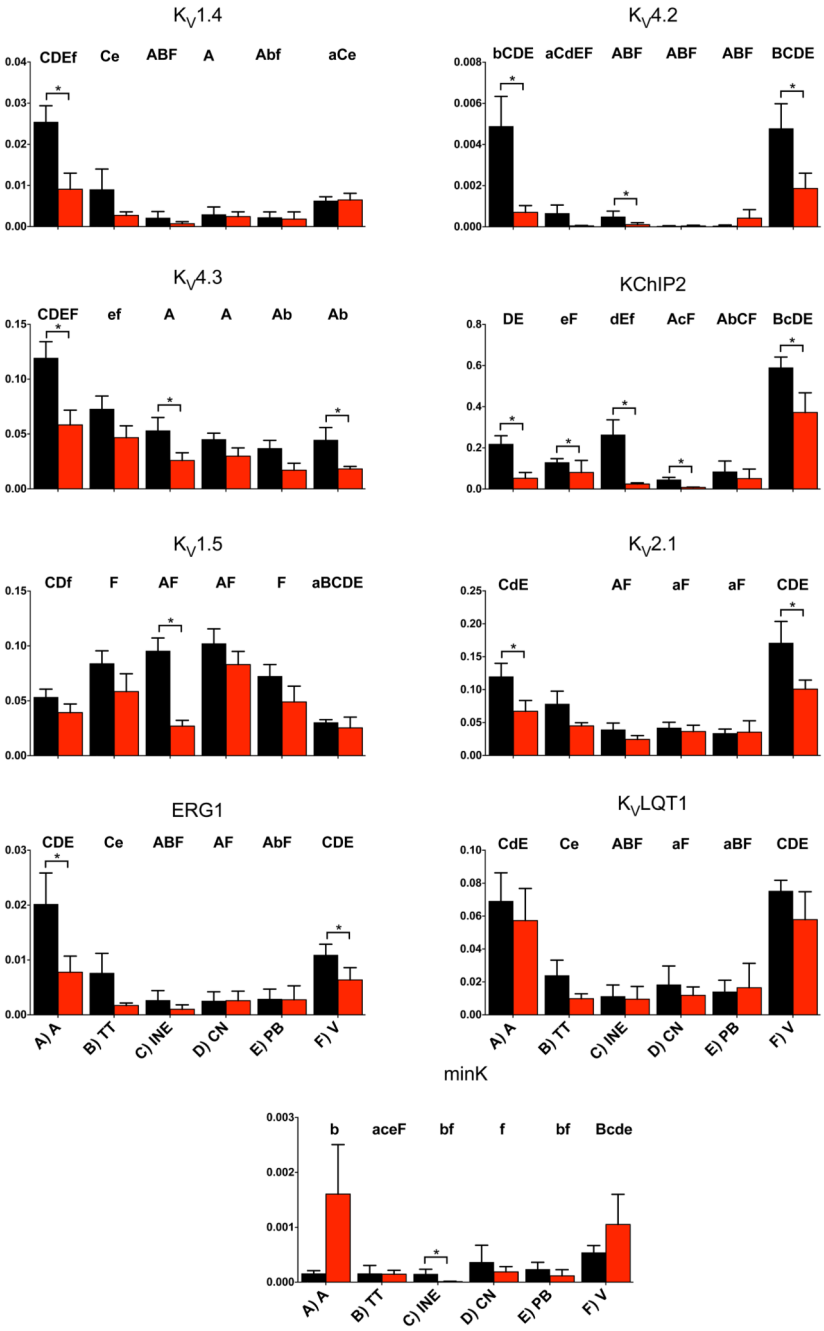

Fig. 5.

Expression of mRNA for voltage-gated K^+ channels.

Europe PMC Funders Author Manuscripts

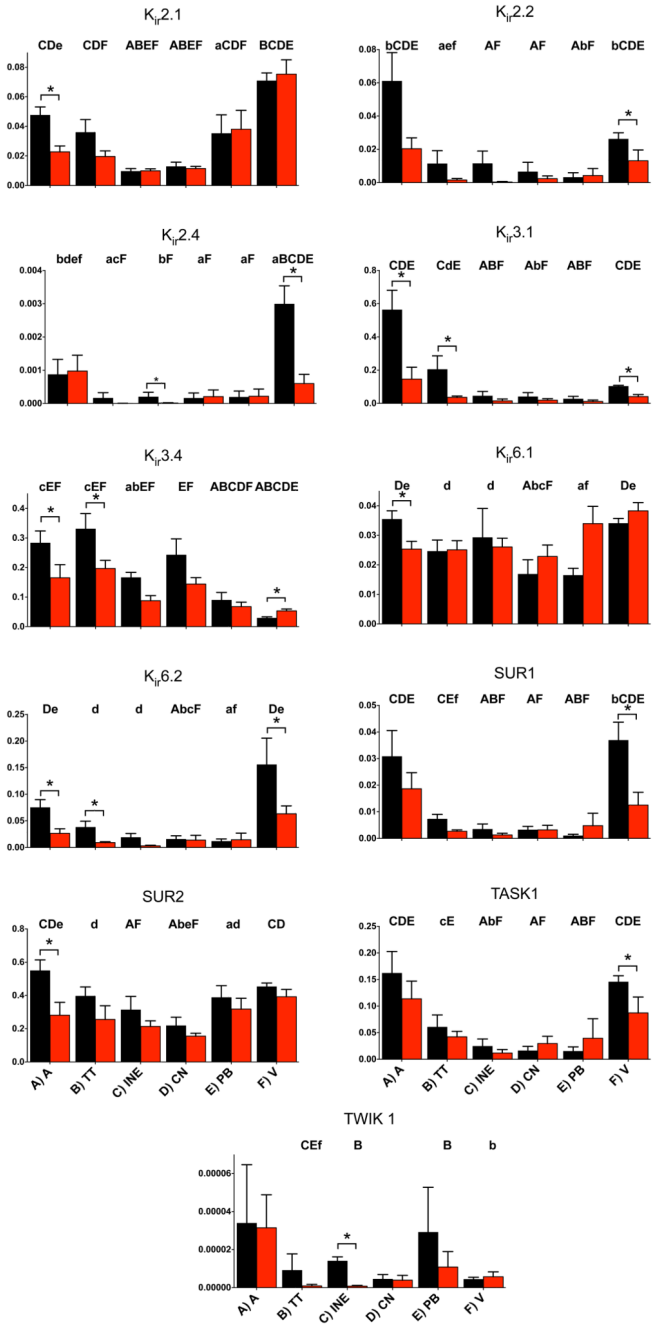

Fig. 6.

Expression of mRNA for inward rectifier K^+ channels.

Europe PMC Funders Author Manuscripts

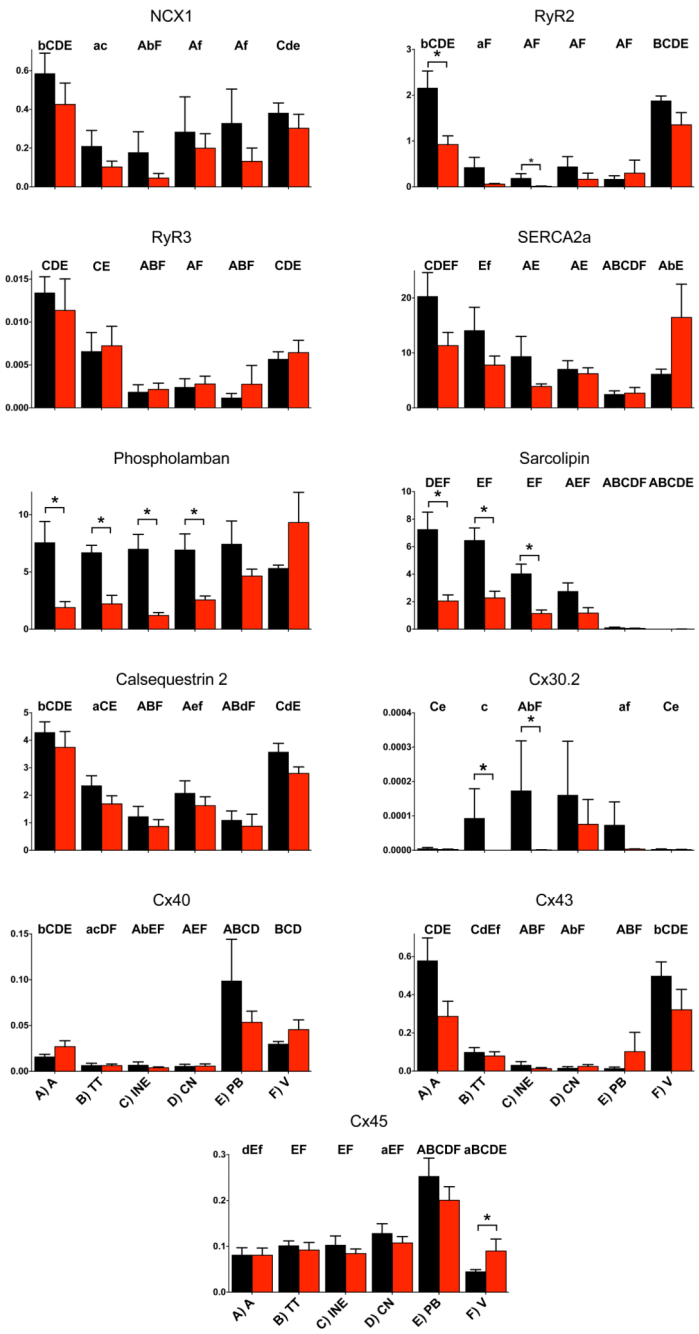

Fig. 7.

Expression of mRNA for Ca^{2+}-handling molecules and connexins.

Europe PMC Funders Author Manuscripts

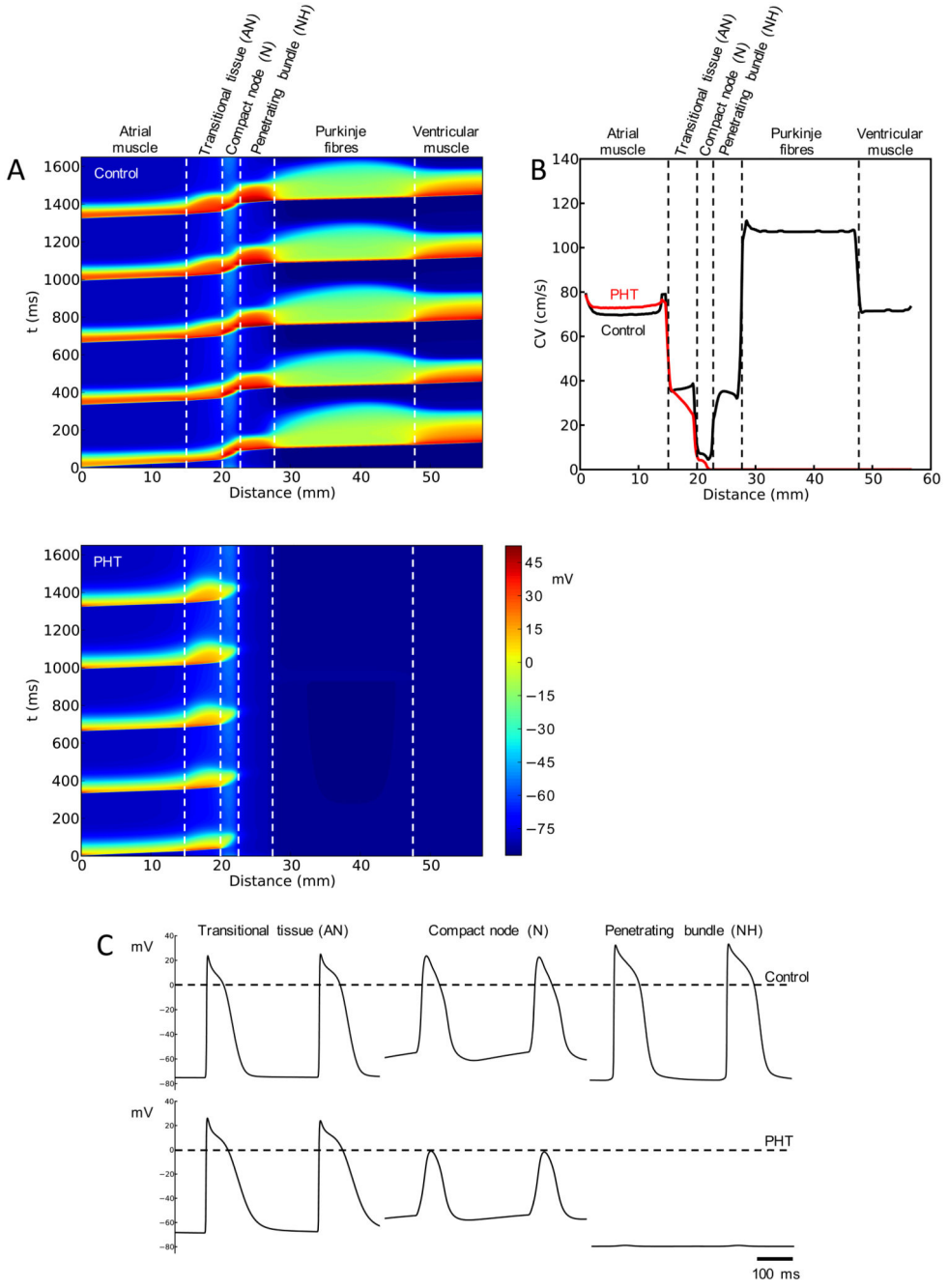

Fig. 8.

Remodelling of AV node predicts heart block in PHT. A, simulated conduction along AV conduction axis under control conditions (top) and in PHT (bottom). Propagation of five consecutive action potentials shown. Membrane potential (colour coded) is shown as a function of time and distance. B, computed conduction velocity (CV) along AV conduction axis under control conditions and in PHT. C, computed action potential profiles along AV conduction axis under control conditions and in PHT.

Europe PMC Funders Author Manuscripts

Table 1

Body, heart and lung weights at day 0, day 21 and day of sacrifice and echocardiography and ECG parameters on day of sacrifice. Data are presented as mean±SEM. Differences between monocrotaline-injected and control rats assessed by Student's *t*-test; *significantly different from control data. LV, left ventricle; PAAD, pulmonary artery acceleration time; PAD, pulmonary artery deceleration; PVmax, maximum pulmonary artery velocity; RV, right ventricle.

	Control rats	PHT rats	P value
Body, heart and lung weights			
Body weight at day 0 (g; n=8/8)	208±9	208±5	0.9897
Body weight at day 21 (g; n=8/8)	299±13	277±7	0.1573
Body weight on day of termination (g; n=8/8)	308±15	270±8*	0.0446
Heart weight (g; n=6/8)	1.6±0.1	1.9± 0.1*	0.0239
Heart:body weight ratio (n=6/8)	0.0050±0.0004	0.0070±0.0003*	0.0010
Lung weight (g; n=8/8)	1.4±0.1	2.7±0.2*	<0.0001
Lung:body weight ratio (n=8/8)	0.0050±0.0003	0.0100±0.0009*	0.0001
Echocardiography parameters			
LV septal wall thickness, diastole (cm; n=8/8)	0.15±0.01	0.18±0.01	0.1978
LV internal diameter, diastole (cm; n=8/8)	0.71±0.03	0.44±0.05*	0.0002
LV posterior wall, diastole thickness (cm; n=8/8)	0.18±0.01	0.20±0.01	0.3874
LV septal wall thickness, systole (cm; n=8/8)	0.26±0.02	0.30±0.02	0.1275
LV internal diameter, systole (cm; n=8/8)	0.36±0.03	0.17±0.03*	0.0004
LV posterior wall, systole thickness (cm; n=8/8)	0.27±0.01	0.29±0.02	0.3719
PAAT (ms; n=8/8)	33.0±3.6	14.3±0.6*	0.0001
PAD (m/s; n=8/8)	14.9±1.7	33.6±3.5*	0.0003
PVmax (m/s; n=8/8)	1.09±0.05	0.70±0.05*	<0.0001
RV wall thickness, diastole (cm; n=8/8)	0.09±0.01	0.14±0.01*	<0.0001
RV internal dimension, diastole (cm; n=8/8)	0.27±0.02	0.38±0.05	0.0598
RV wall thickness, systole (cm; n=8/8)	0.13±0.01	0.16±0.01*	0.0375
RV internal dimension, systole (cm; n=8/8)	0.12±0.02	0.25±0.04*	0.0065
RV fractional shortening (%; n=8/8)	54.4±4.9	34.4±5.1*	0.0131
ECG parameters			
RR interval (ms; n=27/28)	145±2	158±2*	<0.0001
PR interval (ms; n=27/28)	46.1±0.7	45.8±0.7	0.7269
QRS duration (ms; n=27/28)	15.5±0.5	14.7±0.4	0.2309
QT interval (ms; n=27/27)	52±2	103±3*	<0.0001
QTc interval (ms; n=27/27)	136.7±4.1	259.3±6.9*	<0.0001

Europe PMC Funders Author Manuscripts

Table 2

Electrical properties of Langendorff-perfused heart and isolated AV node preparation from control and PHT rats. Data are presented as mean±SEM. Differences between PHT and control rats assessed by Student's *t*-test; Fisher's exact test was used to compare incidences of complete heart block; *significantly different from control data. AERP, atrial effective refractory period; AVERP, AV node effective refractory period; AVFRP, AV node functional refractory period; VERP, ventricular effective refractory period.

	Control rats	PHT rats	P value
Isolated Langendorff-perfused heart			
RR interval (ms; n=9/11)	237±8	244±14	0.6556
PR interval (ms; n=9/11)	43±2	44±2	0.6922
QT interval (ms; n=9/11)	56±5	135±10*	<0.0001
QTc interval (ms; n=9/11)	116±10	275±18*	<0.0001
QRS duration (ms; n=9/11)	13±1	16±3	0.3813
AERP (ms; n=9/9)	34±2	43±5	0.1508
Wenckebach cycle length (ms; n=10/11)	111±3	117±3	0.1640
AVERP (ms; n=10/10)	88±1	94±3*	0.0364
AVFRP (ms; n=10/10)	115±2	122±2*	0.0122
VERP (ms; n=6/4)	40±3	98±11*	0.0003
Isolated right atrium-AV node preparation			
RR interval (ms; n=9/11)	216±10	212±7	0.7143
AH interval (ms; n=10/6)	41±5	53±6	0.1579
Wenckebach cycle length (ms; n=9/5)	129±7	139±11	0.4932
AVERP (200 ms cycle length; n=5/4)	110±13	114±13	0.8113
AVERP (150 ms cycle length; n=6/2)	95±4	102±15	0.5008
AVFRP (200 ms cycle length; n=2/4)	133±1	138±11	0.7759
AVFRP (150 ms cycle length; n=7/2)	117±5	127±6	0.3517
Incidence of complete heart block (%; n=10/12)	0%	50%*	0.015